

# A Framework for Evaluating Security in the Presence of Signal Injection Attacks

Ilias Giechaskiel  
University of Oxford  
ilias.giechaskiel@cs.ox.ac.uk

Youqian Zhang  
University of Oxford  
youqian.zhang@cs.ox.ac.uk

Kasper B. Rasmussen  
University of Oxford  
kasper.rasmussen@cs.ox.ac.uk

**Abstract**—Sensors are embedded in security-critical applications from medical devices to nuclear power plants, but their outputs can be spoofed through signals transmitted by attackers at a distance. To address the lack of a unifying framework for evaluating the effect of such transmissions, we introduce a system and threat model for signal injection attacks. Our model abstracts away from specific circuit-design issues, and highlights the need to characterize the response of Analog-to-Digital Converters (ADCs) beyond their Nyquist frequency. This ADC characterization can be conducted using direct power injections, reducing the amount of circuit-specific experiments to be performed. We further define the concepts of existential, selective, and universal security, which address attacker goals from mere disruptions of the sensor readings to precise waveform injections. As security in our framework is not binary, it allows for the direct comparison of the level of security between different systems. We additionally conduct extensive experiments across all major ADC types, and demonstrate that an attacker can inject complex waveforms such as human speech into ADCs by transmitting amplitude-modulated (AM) signals over carrier frequencies up to the GHz range. All ADCs we test are vulnerable and demodulate the injected AM signal, although some require a more fine-tuned selection of the carrier frequency. We finally introduce an algorithm which allows circuit designers to concretely calculate the security level of real systems, and we apply our definitions and algorithm in practice using measurements of injections against a smartphone microphone. Overall, our work highlights the importance of evaluating the susceptibility of systems against signal injection attacks, and introduces both the terminology and the methodology to do so.

## I. INTRODUCTION

In our daily routine we interact with dozens of sensors: from motion detection in home security systems and tire pressure monitors in cars, to accelerometers in smartphones and heart rate monitors in smartwatches. The integrity of these sensor outputs is crucial, as many security-critical decisions are taken in response to the sensor values. However, it has recently been shown that specially-crafted adversarial signals can be used to remotely induce waveforms into the outputs of sensors, thereby attacking pacemakers [1], temperature sensors [2], smartphone microphones [3], and car-braking mechanisms [4]. These attacks cause a system to report values which do not match the true sensor measurements, and trick it into performing dangerous actions such as raising false alarms, or even delivering defibrillation shocks.

The root cause of these vulnerabilities lies in the unintentional side-effects of the physical components of a system. For example, the wires connecting sensors to microcontrollers

behave like low-power, low-gain antennas, and can thus pick up high-frequency electromagnetic radiations. Although these radiations are considered “noise” from an electrical point of view, hardware imperfections in the subsequent parts of the circuit can “demodulate” attacker injections into meaningful waveforms. Specifically, these radiations are digitized along with the true sensor outputs, which represent a physical property as an analog electrical quantity. This digitization process is conducted by Analog-to-Digital Converters (ADCs), which, when used outside of their intended range, cause noise-like high-frequency signals to be interpreted as meaningful low-frequency signals.

Despite the potential that signal injection attacks have to break security and integrity guarantees, there is no unifying framework for evaluating the effect of such adversarial transmissions. Our work fills this gap through the following contributions:

- 1) We propose a high-level system model, which allows us to abstract away from engineering concerns associated with remote transmissions, such as distance and antenna design (Section II).
- 2) We highlight the importance of testing the response of Analog-to-Digital Converters (ADCs) beyond their Nyquist frequency using direct injections, thus reducing the amount of circuit-specific experiments that need to be performed remotely. We conduct experiments across all major ADC types, and show that they can all demodulate amplitude-modulated (AM) signals. We find that some ADCs require carefully-chosen carrier frequencies to demodulate signals, while, in other cases, ADCs can be vulnerable to transmissions even in the GHz range. These high frequencies allow an adversary to inject waveforms into the ADC, even when the wire connecting the sensor and the ADC is short (Section III).
- 3) We define security against adversarial signal injection attacks. Our definitions address effects ranging from mere disruptions of the sensor readings, to precise waveform injections of attacker-chosen values (Section IV).
- 4) We introduce an algorithm to calculate the security level of a system, and we perform a case-study of “OK Google” command injections into a smartphone microphone to demonstrate the algorithm and our definitions in practice (Section V).

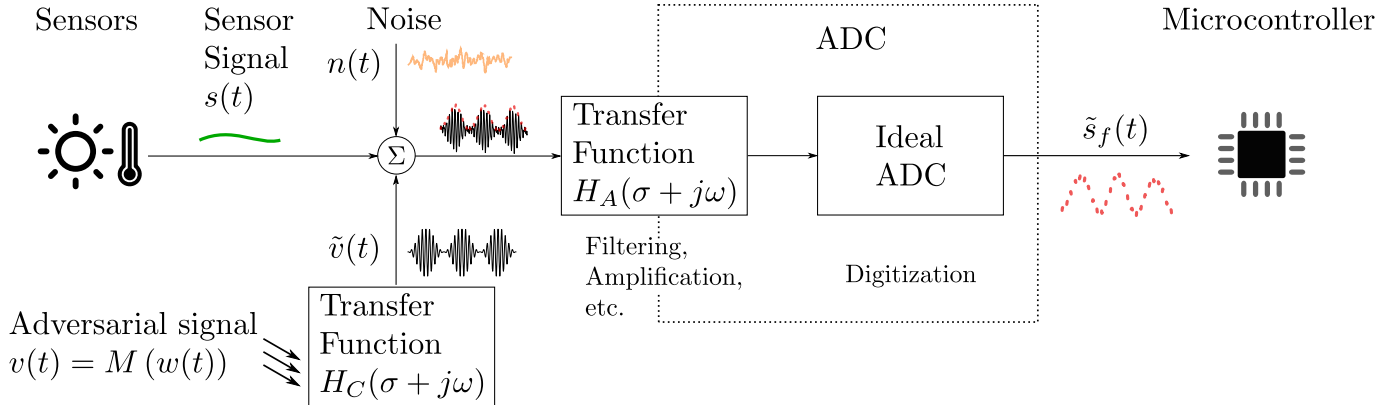


Fig. 1: System model: an adversarial signal  $v(t)$  enters the circuit and is transformed via  $H_C$ . It is digitized along with the sensor signal  $s(t)$  and the noise  $n(t)$  through an ADC-specific transfer function  $H_A$ . If the attack is successful, the digitized signal will contain the demodulated version  $w(t)$  of the attacker signal  $v(t) = M(w(t))$ .

- 5) We discuss how our model can be used to inform circuit design choices, and how to interpret defense mechanisms and other types of signal injection attacks in its context (Section VI).

Overall, our work highlights the importance of testing systems against signal injection attacks, and proposes a model and a methodology to evaluate the security of real devices.

## II. SYSTEM AND ADVERSARY MODEL

Remote signal injection attacks pose new challenges from a threat-modeling perspective, since one should neither simply assume that the adversary can arbitrarily and precisely change any sensor reading, nor should one ignore them entirely. To create a threat model and define security in its context, we need to first abstract away from specific circuit designs and engineering concerns related to remote transmissions. To do so, we separate the behavior of a system into two different transfer functions. The first function describes circuit-specific behavior, including how adversarial signals enter the circuit (e.g., through PCB wires acting as antennas). The second transfer function is ADC-specific, and dictates how the signals which have made it into the circuit are digitized. This model allows us to characterize ADCs independently of the rest of the setup using direct power injections (Section III), reducing the amount of circuit-specific experiments to be performed. We describe this model in greater detail in Section II-A, taking a necessary detour into electrical engineering to show why our proposal makes for a good system model. We then explain some sources of measurement errors even in the absence of an adversary in Section II-B and finish by detailing the capabilities and limitations of the adversary in Section II-C. Both sub-sections are crucial in motivating the security definitions of Section IV.

### A. Circuit Model

Analog-to-Digital Converters (ADCs) are central in the digitization process of converting signals from the analog to the digital realm, and our circuit block diagram (Figure 1)

reflects that. In the absence of an adversary, the ADC digitizes the sensor signal  $s(t)$  as well as the environmental noise  $n(t)$ , and transfers the digital bits to a microcontroller. We model the ADC in two parts: an “ideal” ADC which simply digitizes the signal, and a transfer function  $H_A$ . This transfer function describes the internal behavior of the ADC, which includes effects such as filtering and amplification. The digitized version of the signal  $\tilde{s}_f(t)$  depends on both this transfer function, and the sampling frequency  $f$  of the ADC. An adversarial signal can enter the system (e.g., through the wires connecting the sensor to the ADC) and add to the sensor signal and the noise. This process can be described by a second, circuit-specific transfer function  $H_C$ , which transforms the adversarial signal  $v(t)$  into  $\tilde{v}(t)$ . Note that components such as external filters and amplifiers in the signal path between the point of injection and the ADC can be included in either  $H_A$  or  $H_C$ . We include them in  $H_A$  when they also affect the sensor signal  $s(t)$ , but in  $H_C$  when they are specific to the coupling effect.  $H_C$  and  $H_A$  are discussed in detail in Sections II-A1 and II-A2 respectively.

1) *Circuit Transfer Function  $H_C$* : To capture the response of the circuit to external signal injections, we introduce a transfer function  $H_C$ . This transfer function explains why the adversarial waveforms must be modulated, and why it is helpful to try and reduce the number of remote experiments to perform. For electromagnetic interference (EMI) attacks, the wires connecting the sensor to the ADC pick up signals by acting as (unintentional) low-power, low-gain antennas, which are resonant at specific frequencies related to the inverse of the wire length [5]. Non-resonant frequencies are attenuated more, so for a successful attack the adversary must transmit signals at frequencies with relatively low attenuation. For short wires, these frequencies are in the GHz range [5], so the low-frequency waveform  $w(t)$  that the adversary wants to inject into the output of the ADC  $\tilde{s}_f(t)$  may need to be modulated over a high-frequency carrier. We denote this modulated version of the signal by  $v(t)$ .

$H_C$  is also affected by passive and active components on

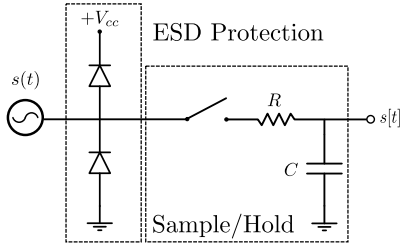


Fig. 2: The sample-and-hold mechanism of an ADC is an  $RC$  low-pass filter. Electrostatic Discharge (ESD) protection diodes can result in non-linearities of the input signal.

the path to the ADC, and can also be influenced by inductive and capacitive coupling for small transmission distances, as it closely depends on the circuit components and their placement. Specifically, it is possible for 2 circuits with “the same components, circuit topology and placement area” to have different EMI behavior depending on the component placement on the board [6]. Despite the fact that it is hard to mathematically model and predict the behavior of circuits in response to different signal transmissions,  $H_C$  can still be determined empirically using frequency sweeps. It presents a useful abstraction, allowing us to separate the behavior of the ADC (which need only be determined once, for instance by the manufacturer) from circuit layout and transmission details.

Note, finally, that  $H_C$  can also account for defense mechanisms, as we further discuss in Section VI. For example, shielding increases the attenuation factor of  $H_C$ .  $H_C$  can also account for distance factors between the adversary and the circuit under test: due to the Friis transmission formula, as distance doubles, EMI transmission power needs to quadruple, each time increasing attenuation by 6 dB. This allows us to side-step engineering issues of remote transmissions and reduce the number of parameters used in our security definitions of Section IV.

2) *ADC Transfer Function  $H_A$* : Every system with sensors contains one or more ADCs, which may even be integrated into the sensor chip itself. ADCs are not perfect, but contain components which may cause there to be a mismatch between the “true” value at the ADC input and the digitized output. In this section, we describe how these components affect the digitization process, which allows us to reason about the experimental results of Section III.

Specifically, although there are many types of ADCs, every ADC contains three basic components: a “sample- or track-and-hold circuit where the sampling takes place, the digital-to-analog converter and a level-comparison mechanism” [7]. The sample-and-hold component acts as a low-pass-filter, and makes it harder for an adversary to inject signals modulated at high frequencies. However, the level-comparison mechanism is essentially an amplifier. This amplifier has non-linearities, which induce DC offsets, and allow low-frequency intermodulation products to pass through. These ADC-specific transformations, modeled through  $H_A$ , unintentionally demodulate high-frequency signals which are not attenuated by  $H_C$ .

**Sample-And-Hold Filter Characteristics:** A sample-and-hold (S/H) mechanism is a simple  $RC$  circuit connected to the analog input, with the resistor and the capacitor connected in series (Figure 2). The transfer function of the voltage across the capacitor is  $H_{S/H}(j\omega) = \frac{1}{1+j\omega RC}$ , and the magnitude of the gain is  $G_{S/H} = \frac{1}{\sqrt{1+(\omega RC)^2}}$ . As a result, as the angular frequency  $\omega = 2\pi f$  increases, the gain is reduced: the S/H mechanism acts as a low-pass filter. The  $-3$  dB cutoff frequency is thus  $f_{cut} = \frac{1}{2\pi RC}$ , which is often much higher than the sampling rate of the ADC (Section III, Table I). Hence, “aliasing” occurs when signals beyond the Nyquist frequency are present at the input of the ADC: high-frequency signals become indistinguishable from low-frequency signals which the ADC can sample accurately.

**Amplifier Non-Linearities:** Every ADC contains amplifiers: a comparator, and possibly buffer and differential amplifiers. Many circuits also contain additional external amplifiers to make weak signals measurable. All these amplifiers have harmonic and intermodulation non-linear distortions [8], which an adversary can exploit. Harmonics are produced when an amplifier transforms an input  $v_{in}$  to an output  $v_{out} = \sum_{n=1}^{\infty} a_n v_{in}^n$ . In particular, if  $v_{in} = \hat{v} \cdot \sin(\omega t)$ , then:

$$v_{out} = \left( \frac{a_2 \hat{v}^2}{2} + \frac{3a_4 \hat{v}^4}{8} + \dots \right) + (a_1 \hat{v} + \dots) \sin(\omega t) - \left( \frac{a_2 \hat{v}^2}{2} + \dots \right) \cos(2\omega t) + \dots$$

This equation shows that “when nonlinear circuits are excited with a single sinusoidal signal, the frequency spectrum of the output contains a spectral component at the original (fundamental) frequency, as well as spectral components at multiples of the fundamental frequency (harmonic frequencies)” [8]. Moreover, the output includes a DC component, which depends only on the even-order non-linearities of the system. Besides harmonics, intermodulation products arise when the input signal is a sum of two sinusoids (for instance when the injected signal sums with the sensor signal):  $v_{in} = \hat{v}_1 \cdot \sin(\omega_1 t) + \hat{v}_2 \cdot \sin(\omega_2 t)$ . In that case, the output signal contains frequencies of the form  $n\omega_1 \pm m\omega_2$  for integers  $n, m \neq 0$ . These non-linearities demodulate attacker waveforms, even when they are modulated on high-frequency carriers.

**Diode Rectification:** Figure 2 shows that the input to ADC can contain reverse-biased diodes to ground and  $V_{cc}$  to protect the input from Electrostatic Discharge (ESD). When the input to the ADC is negative, or when it exceeds  $V_{cc}$ , the diodes clamp it, causing non-linear behavior. When the sensor signal  $s(t)$  is positive, this behavior is also asymmetric, causing a DC shift [8], which compounds with the amplifier non-linearities.

**Conclusion:** All ADCs contain the same basic building blocks, which we model through  $H_A$ . We expect the sample-and-hold mechanism to severely attenuate high-frequency signals beyond the maximum sampling rate of the ADC. We also expect non-linearities due to ESD diodes and amplifiers in the ADC to cause DC offsets and the demodulation of signals through harmonics and intermodulation products.

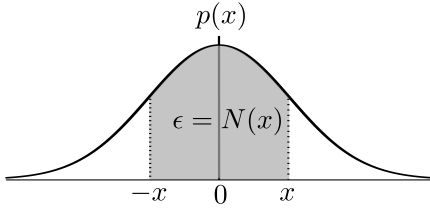


Fig. 3: Noise probability distribution  $p(x)$ . The shaded area represents the probability  $\epsilon = N(x) = \Pr[|n(t)| \leq x]$ .

### B. Sampling Errors in the Absence of an Adversary

Even in the absence of an adversary, the digitization process through ADCs entails errors. For a successful attack, the adversary must change sensor readings by more than the amount of error that is typical for a given application. In our model, we account for two main error sources: quantization error in the ADC and environmental noise.

Quantization errors exist due to the inherent loss of accuracy in the sampling process. An ADC can only represent values within a range, say between  $V_{min}$  and  $V_{max}$  volts. An ADC also has a finite binary representation, say of  $N$  bits, called the *resolution* of the ADC. Every value between  $V_{min}$  and  $V_{max}$  is mapped to one of the  $2^N$  values that can be represented using  $N$  bits. As a result, there is a *quantization error* between the true sensor analog value  $s$  and the digitized value  $\tilde{s}$ . The maximum value of this error is

$$Q = \frac{V_{max} - V_{min}}{2^{N+1}} \geq |s - \tilde{s}| \quad (1)$$

The second source of error comes from environmental noise, which may affect measurements. We assume that this noise, denoted by  $n(t)$ , is independent of the signal being measured, and that it comes from a zero-mean distribution, i.e., that the noise is *white*. The security definitions we introduce in Section IV require an estimate of the level of noise in the system, so we introduce some relevant notation here. We assume that  $n(t)$  follows a probability distribution function (PDF)  $p(x)$ , and define  $N(x)$  as the probability that the noise is between  $-x$  and  $x$ , as shown in Figure 3, i.e.,

$$N(x) = \Pr[|n(t)| \leq x] = \int_{-x}^x p(u) du$$

Note that typically the noise is assumed to come from a normal distribution (“Additive White Gaussian Noise (AWGN)”), but this assumption is not necessary in our models and definitions.

We are also interested in the inverse of this function, where given a probability  $0 \leq \epsilon < 1$ , we want to find  $x \geq 0$  such that  $N(x) = \epsilon$ . For this  $x$ , the probability that the noise magnitude falls within  $[-x, x]$  is  $\epsilon$ , as also shown in Figure 3. Because for some distributions there might be multiple  $x$  for which  $N(x) = \epsilon$ , we use the smallest such value:

$$N^{-1}(\epsilon) = \inf\{x \geq 0 : N(x) = \epsilon\} \quad (2)$$

Since  $N(x)$  is an increasing function, so is  $N^{-1}(\epsilon)$ .

To account for repeated measurements, we introduce a short-hand for sampling errors, which we denote by  $E_s(t)$ .

The sampling errors depend on the sensor input into the ADC  $s(t)$ , the sampling rate  $f$ , the discrete output of the ADC  $\tilde{s}_f(t)$  as well as the conversion delay  $\tau$ , representing the time the ADC takes for complete a conversion:

$$E_s(t) = \begin{cases} |\tilde{s}_f(t + \tau) - s(t)| & \text{if a conversion starts at } t \\ 0 & \text{otherwise} \end{cases} \quad (3)$$

### C. Adversary Model

Our threat model and definitions can capture all attacker goals, from attackers who merely want to disrupt sensor outputs, to those who wish to inject precise waveforms into a system. We define these notions precisely in Section IV, but here we describe the attacker capabilities based on our model of Figure 1. Specifically, in our model, the adversary can only alter the transmission signal  $v(t)$ . He/she cannot directly influence the sensor signal  $s(t)$ , the (residual) noise  $n(t)$ , or the transfer functions  $H_A$  and  $H_C$ . The adversary knows  $H_A$ ,  $H_C$ , and the distribution of the noise  $n(t)$ , although the true sensor signal  $s(t)$  might be hidden from the adversary (see Section IV-B). The only constraint placed on the adversarial signal is that the attacker is only allowed to transmit signals  $v(t)$  whose peak voltage level is bounded by some constant  $V_{PK}^{Adv}$ , i.e.,  $|v(t)| \leq V_{PK}^{Adv}$  for all  $t$ . We call this adversary a  $V_{PK}^{Adv}$ -bound adversary, and all security definitions are against such bounded adversaries.

We choose to restrict voltage rather than restricting power or distance, as it makes for a more powerful adversarial model. Our model gives the adversary access to any physical equipment necessary (such as powerful amplifiers and highly-directional antennas), while reducing the number of parameters needed for our security definitions of Section IV. Distance/power effects can be compensated directly through altering  $V_{PK}^{Adv}$ , or indirectly by integrating them into  $H_C$ , as discussed in Section II-A1.

## III. DETERMINING RESILIENCE TO MALICIOUS SIGNALS

As explained in Section II, an adversary trying to inject signals remotely into a system typically needs to transmit modulated signals over high-frequency carriers. The vulnerability of a system is thus dependent on both the ADC behavior (described by  $H_A$ ) and the circuit-specific behavior due to  $H_C$ . As  $H_C$  is unique to each circuit and needs to be re-calculated even for minor changes to its components and layout [9], the first step to determine the system vulnerability is to understand the behavior of the ADC used.

In this section, we explore the behavior of ADCs by injecting signals of variable frequencies into different types of ADCs. We explain our setup of direct power injections in Section III-A. In Section III-B, we describe in detail the behavior exhibited by the ADC of the popular ATmega328P chip by Atmel under different experimental conditions. We finally summarize our findings for other ADCs in Section III-C, which shows that all ADCs are vulnerable to signal injections due to non-linearities in their components.

ADC	Manufacturer	Form	Type	Bits	Max $f_s$	Eff. $f_s$	$R$	$C$	$f_{cut}$
TLC549	Texas Instruments	DIP	SAR	8	40 kHz	29 kHz	1 k $\Omega$	60 pF	2.7 MHz
ATmega328P	Atmel	Integrated	SAR	10	†76.9 kHz	8.3 kHz	1-100 k $\Omega$	14 pF	0.1-11.4 MHz
Artix7	Xilinx	Integrated	SAR	12	1 MHz	198 kHz	10 k $\Omega$	3 pF	5.3 MHz
AD7276	Analog Devices	TSSOP	SAR	12	3 MHz	35 kHz	75 $\Omega$	32 pF	66.3 MHz
AD7783	Analog Devices	TSSOP	$\Delta\Sigma$	24	19.79 Hz	19.71 Hz	N/A	N/A	[50,60 Hz]
AD7822	Analog Devices	DIP	Flash	8	2 MHz	84 kHz	310 $\Omega$	4 pF	128.4 MHz

TABLE I: Parameters of the ADCs used in our experiments, which were selected to cover different properties. See text for details. †The ATmega328P maximum sampling rate is only 15 kHz at maximum resolution.

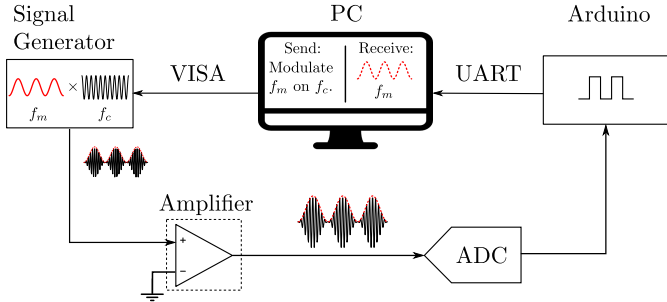


Fig. 4: Experimental setup. Signals are directly injected into the ADC, with or without an amplifier.

#### A. Setup and Methodology

Our experimental setup uses direct power injections into the ADCs for reproducibility and is illustrated in Figure 4. A PC is used to both control the signal generation process, and to record measurements from different ADCs. The signals we transmit are generated via a Rohde & Schwarz SMC100A/B103 signal generator over the Virtual Instrument Software Architecture (VISA) interface. We chose to use this signal generator instead of lower-cost Software-Defined Radio (SDR) platforms to ensure that the signals produced are clean and that the Spurious-Free Dynamic Range (SFDR) is minimized.<sup>1</sup> The ADCs (except for the Artix 7 FPGA) are controlled using an Arduino, and measurements are transferred to the PC over the serial UART interface. In most experiments, the output of the signal generator is connected to the ADC input directly, although for some experiments we additionally use an external amplifier between the generator and the ADC to test the effect of the amplifier non-linearities.

The 6 ADCs used for our experiments were selected to cover a range of different properties. They come from 4 manufacturers (Texas Instruments, Analog Devices, Atmel, Xilinx) in different forms (integrated into other ICs, or standalone surface-mount or dual-in-line chips) and are controlled via different protocols. The maximum sampling rate  $f_s$  of the ADCs ranges from a few Hz to several MHz, while the resolution ranges from 8 to 24 bits. We have also chosen to use ADCs with different sampling/conversion techniques (“ADC type”), including Delta-Sigma ( $\Delta\Sigma$ ), half-flash, and

<sup>1</sup>According to the generator’s specifications, the frequency error is  $< 10^{-7}$ , and the decibels relative to the carrier are  $< -30$  dBc.

successive approximation (SAR). The properties of the ADCs used are summarized in Table I.

Table I additionally specifies the series resistance  $R$  and capacitance  $C$  of the sample-and-hold circuit of the ADCs (Figure 2), as noted in their respective datasheets. The AD7783 datasheet does not give  $R, C$  parameters for its input, but it includes notch filters to reject 50 and 60 Hz signals (for AC mains hum suppression). We have further calculated the  $-3$  dB cutoff frequency  $f_{cut}$  based on the  $R, C$  parameters and the equations of Section II-A2. Note that as the ADCs are controlled with an Arduino and the measurements are transferred over UART, the effective sampling rate is lower than the maximum sampling rate, and is reported separately in Table I as “Eff.  $f_s$ ”.

In our tests, we inject sinusoidal signals of different frequencies  $f_m$ , which have been amplitude modulated (AM) on different carrier frequencies  $f_c$ . We also vary the modulation depth  $m$  and the transmission power  $P$  (equivalently, the peak voltage). In other words, we consider the intended signal to be  $w(t) = \sin(2\pi f_m t)$ , the sensor signal to be absent ( $s(t) = 0$ ), and we want to evaluate how “close”  $w(t)$  is to the ADC output  $\tilde{s}_f(t)$ . The closer  $w(t)$  is to  $\tilde{s}_f(t)$  at high frequencies, the more vulnerable a system is to signal injection attacks, as an adversary can transmit modulated signals, which then get unintentionally demodulated by the ADC.

To measure how close signals are (and therefore how effective injections are), we use Pearson’s correlation coefficient (PCC)  $\rho$ , which is commonly found in signal-alignment and optimization applications [10], [11]. PCC is a good similarity metric, as it removes the mean value of the compared signals (DC shift, in our case), and the effect of scaling (which relates to transmission power). As PCC is sensitive to phase offset, we first find the time lag between the ideal signal  $\tilde{s}_f(t)$  and the measured signal  $w(t)$  through cross-correlation (the signals are aligned when the cross-correlation coefficient is maximized):

$$\text{similarity}(w, \tilde{s}_f) = \rho(w, \tilde{s}_f^{lag}) \quad (4)$$

#### B. ATmega328P Characterization

In this section, we present detailed results for the ADC integrated into the ATmega328P chip by Atmel, which is used in the popular Arduino platform. We test the chip in three different arrangements: the chip on its own, the chip with an amplifier, and the chip with an antenna. Our experimental results support the theoretical model of Section II-A and show that:

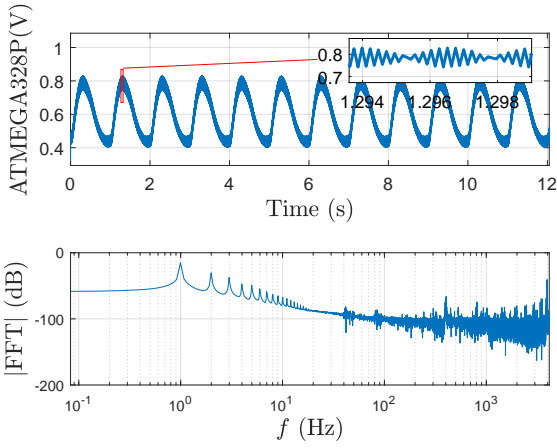
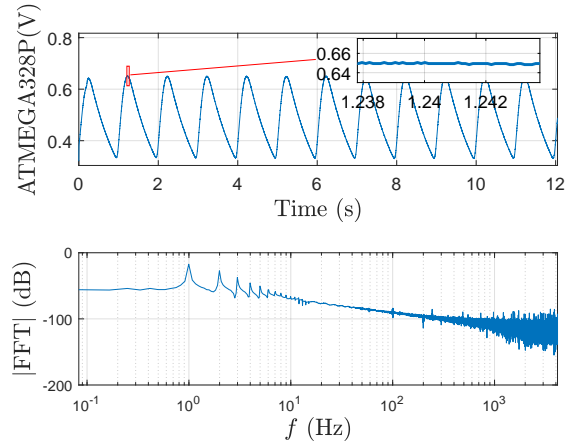
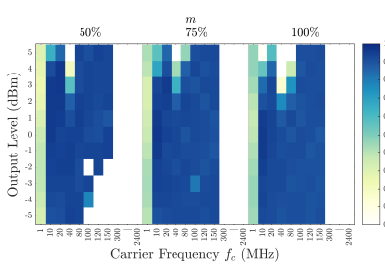
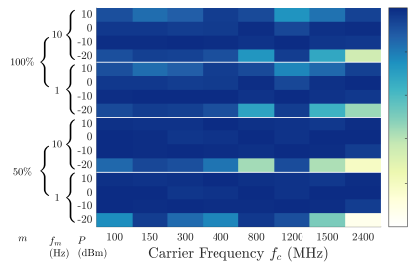
(a)  $f_c = 10$  MHz(b)  $f_c = 80$  MHz

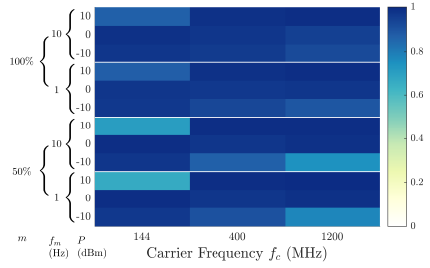
Fig. 5: Example ATmega328P output for power  $P = 0$  dBm, signal frequency  $f_m = 1$  Hz, and modulation depth  $m = 50\%$ . The signal exhibits the correct fundamental frequency, but also contains strong harmonics and a high-frequency component, which is attenuated as the carrier frequency  $f_c$  increases.



(a) ADC only



(b) ADC + Amplifier



(c) ADC + Amplifier + Antenna

Fig. 6: Similarity metrics for injections into the ATmega328P for different transmission powers  $P$ , modulation depths  $m$ , and carrier frequencies  $f_c$ . The amplifier increases the vulnerable frequencies to the GHz range, allowing remote attacks.

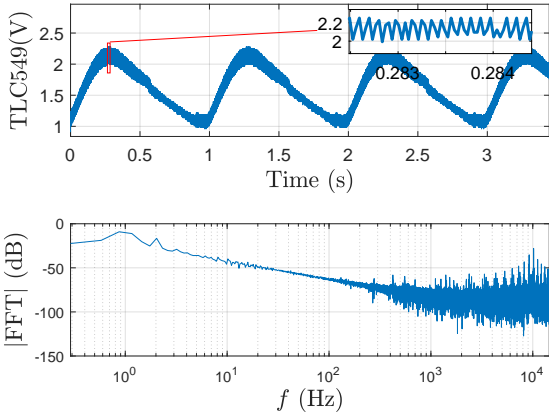
- 1) Non-linearities in the ADC demodulate the transmitted signal, allowing an attacker to inject sinusoidal signals into the system.
- 2) The ADC exhibits a low-pass filtering behavior, but the ADC demodulates signals carried at frequencies multiple times the cut-off frequency of the sample-and-hold mechanism.
- 3) Amplifier non-linearities increase the vulnerable frequency range into the GHz range.
- 4) Our direct injection methodology is a good way of predicting the behavior of the ADC even under remote injection attacks.

**ATmega328P Only:** The first set of experiments target the ATmega328P directly, without using any additional components. Two example measurements of outputs of the ATmega328P, both in the time domain and in the frequency domain are shown in Figure 5. The input to the ADC is a  $f_m = 1$  Hz signal modulated over different high-frequency carriers. As shown in the frequency domain (bottom of Figure 5), the fundamental frequency  $f_m$  dominates all other frequencies, so the attacker is able to inject a signal of the intended frequency into the

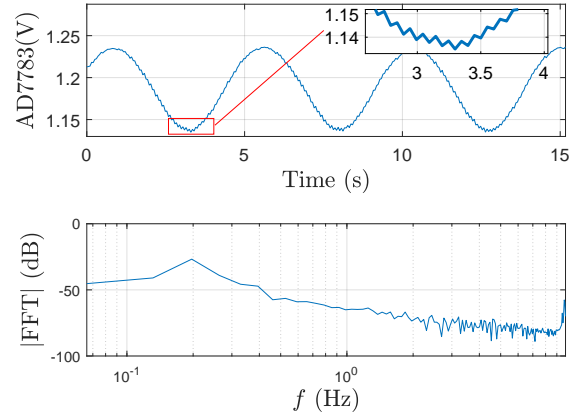
output of the ADC.

However, the output at both carrier frequencies has strong harmonics at  $2f_m, 3f_m, \dots$  Hz, which indicates that the resulting signal is not pure. Moreover, there is a residual high-frequency component, which is attenuated as the carrier frequency  $f_c$  increases. Finally, there is a frequency-dependent DC offset caused, in part, by the ESD diodes, while the peak-to-peak amplitude of the measured signal decreases as the carrier frequency increases, due to the low-pass filtering behavior of the sample-and-hold mechanism.

To evaluate how close the injected signal is to the ideal signal, we calculate the similarities for different transmission powers, modulation depths, and signal frequencies using Equation (4). We fix  $f_m = 1$  Hz, and summarize the results in Figure 6a. For any output power  $P$  and modulation depth  $m$ , the similarity for  $f_c = 1$  MHz is always low due to aliasing. Similarity is high for  $f_c$  between 10 – 150 MHz, but signals are severely attenuated for  $f_c \geq 300$  MHz. Small modulation depths and powers do not result in demodulated outputs, while too much power causes the ADC to be saturated. This leads to partial clipping of the signal, or induces a DC offset



(a) TLC549:  $f_c = 80$  MHz,  $m = 50\%$ ,  $f_m = 1$  Hz



(b) AD7783:  $f_c = 40$  MHz,  $m = 100\%$ ,  $f_m = 10$  Hz

Fig. 7: Example TLC549 and AD7783 outputs for a transmission power of  $P = 5$  dBm. Both ADCs demodulate the injected signal, but present harmonics and some high-frequency components. The AD7783 signal is aliased.

which is beyond the range of the ADC. Overall, the adversary has a range of choices for  $P$  and  $m$ , and can use carrier frequencies which are multiple times the cutoff frequency of the ADC, provided these are not attenuated by the circuit-specific transfer function  $H_C$ .

**ATmega328P + Amplifier:** We further test the behavior of the ADC when using an amplifier, effectively changing  $H_A$ . We use a low-cost, off-the-shelf wideband Low-Noise Amplifier (LNA), whose working range is 1 – 2000 MHz, and can perform a maximum amplification of 32 dB. The amplifier can output at most 10 dBm, and has a noise figure of approximately 2 dB.

We inject signals to the ATmega328P (through the amplifier) on carrier frequencies from 100 MHz to 2.4 GHz at transmission powers between  $-20$  and 10 dBm. We test sine signals of 1 Hz and 10 Hz, and modulate them at 50% and 100% depth. As can be seen in Figure 6b, the similarity is high across all frequencies, provided the transmission power is above a minimum threshold. Clearly, an amplifier before the ADC (and thus before its low-pass filtering effect) makes the ADC vulnerable across any carrier frequency for  $P \geq -10$  dBm. Thus, an amplifier (a) reduces the power requirements for the adversary, and (b) increases the range of vulnerability.

This expanded range also includes GHz signals, allowing an attacker to target systems with short wires between the ADC and the sensor with a lower power budget: short wires are not a sufficient defense against electromagnetic interference attacks. Moreover, we note that an attacker gains an advantage by not obeying the amplifier constraints: abusing the amplifier by transmitting higher-powered signals, or by driving frequency signals outside of the intended range still results in recognizable output. In other words, although the signal may be distorted, the non-linearities still produce outputs within the range of the ADC (also see Section VI).

**ATmega328P + Amplifier + Antenna:** We finally verify that

our ADC characterization through direct power injection is a good predictor for the behavior of remote attacks, while also avoiding engineering and legal issues surrounding remote wireless transmissions. We do so by changing the circuit-specific transfer function  $H_C$  by using antennas both for the attacker transmissions and the amplifier input. We use two Ettus Research omnidirectional VERT400 Antennas, which work at 144 MHz, 400 MHz, and 1.2 GHz. The first antenna is connected to the output of the signal generator, while the second one is connected to the input of the amplifier which is in turn connected to the Arduino.<sup>2</sup> The antennas are placed in parallel at a distance of 5 cm to one another, and the results for sine signals of 1 Hz and 10 Hz are presented in Figure 6c.

The results are similar to those of the previous experiment using just the amplifier: injections are successful for all three frequencies, despite the different setup. Although the minimum power required for successful injections is higher due to transmission losses, the system remains vulnerable due to the amplifier and ADC non-linearities.

### C. Generalizing to Other ADCs

In this section we start by making some ADC-specific comments for the 5 remaining chips we tested. Although we repeated tests for different combinations of the experimental parameters, for brevity we only comment on some specific examples highlighting the differences from the ATmega328P. We then make general remarks based on our observations and the theory of Section II.

**TLC549:** The results for the TLC549 are similar to those of the ATmega328P: the TLC549 also demodulates the injected signal, but still contains harmonics as well as a smaller high-frequency component. An example measurement is shown in Figure 7a.

<sup>2</sup>The amplifier is crucially on the Arduino end, and not on the transmitter end, since in that case the non-linearities would be attenuated and not be transmitted/received by the Arduino antenna.

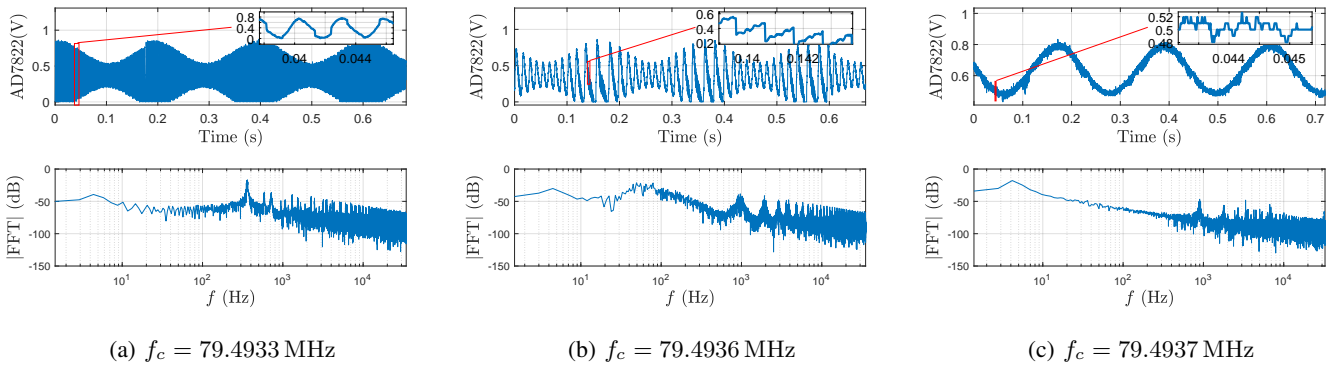


Fig. 8: Example AD7822 output for power  $P = -5$  dBm, signal frequency  $f_m = 5$  Hz, and modulation depth  $m = 50\%$ . The signal is only demodulated for fine-tuned  $f_c$ .

**AD7783:** As the AD7783 only has a sampling frequency of  $f_s = 19.79$  Hz, aliasing occurs when the baseband signal exceeds the Nyquist frequency  $f_s/2$ . For example, when the baseband frequency is  $f_m = 10$  Hz, the fundamental frequency dominating the measurements is of frequency  $2f_m - f_s = 20 - 19.79 = 0.21$  Hz, with a high-frequency component of  $f_s - f_m = 9.79$  Hz. This example is shown in Figure 7b.

**AD7822, AD7276, Artix7:** The three remaining ADCs contain strong high-frequency components which dominate the low-frequency signal. Their outputs thus still appear to be AM-modulated, but at a carrier frequency which is below the ADC's Nyquist frequency. However, with manual tuning of the carrier frequency, it is possible to remove this high frequency component, in effect causing the ADC to demodulate the input as with the previous ADCs. This is shown for the Flash ADC AD7822 in Figure 8, where we change the carrier frequency  $f_c$  in steps of 100 Hz.

**Conclusion:** The results of our experiments lead to the following observations:

- 1) **Generality** – We have verified that all 6 ADCs tested are vulnerable to signal injections at multiple carrier frequencies, as they demodulate signals due to nonlinearities in their components. We experimented with ADCs of all major types and a range of different resolutions and sampling frequencies, and our results matched the theoretical expectations of Section II-A. The issues identified are thus not specific to the chips we used, and should persist for other ADCs as well.
- 2) **Reproducibility** – Most of our experiments did not use additional components or matching circuitry, corresponding to an identity circuit-transfer function  $H_C(\sigma + j\omega) = \mathcal{L}\{\tilde{v}(t)\}/\mathcal{L}\{v(t)\} = 1$ . In other words, the transmitted signal  $v(t)$  and the transformed signal  $\tilde{v}(t)$  (Figure 1) were considered to be equal. When we changed  $H_C$  by performing remote injections, we reached similar conclusions regarding the vulnerability of the system. Our results thus show that an adversary who has characterized the ADC response for different carrier frequencies through direct injections can then experimentally

determine the true, circuit-specific  $H_C$ . This can be done through frequency sweeps, and the adversary can choose to transmit at frequencies and power levels which are not attenuated by either  $H_A$  or  $H_C$ .

- 3) **Low-Pass Filter** – We expected the low-pass filtering behavior of the Sample-and-Hold mechanism (Section II-A2) to reduce the vulnerability of devices to signal injections. However, we found that although all ADCs did exhibit low-pass filtering characteristics, the maximum vulnerable carrier frequency for a given power level was multiple times the cut-off frequency of the  $RC$  circuit at the input of the ADC. This extended the frequency range that an attacker could use for transmissions to attack the system.
- 4) **Power** – The adversary needs to select the power level of transmissions carefully: too much power in the input of the ADC can cause saturation and/or clipping of the measured signal. Too little power, on the other hand, results in output that looks like noise or a zero signal.
- 5) **Carrier Frequency** – The carrier frequencies which could be used to attack an ADC differed considerably. Some ADCs were vulnerable at any carrier frequency that is not severely attenuated by the sample-and-hold mechanism. For others, high-frequency components dominated the intended baseband signal of frequency  $f_m$  in the ADC output for most frequencies. However, even for those ADCs, carefully-chosen carrier frequencies resulted in a demodulated ADC output and high similarity values, even if only for a few seconds.<sup>3</sup>

#### IV. SECURITY DEFINITIONS

Having understood the behavior of ADCs beyond their Nyquist frequency, we can now define security in the presence of signal injection attacks. In our system and adversary model of Figure 1, the  $V_{PK}^{Adv}$ -bound adversary is allowed to transmit any waveform  $v(t)$ , provided that  $|v(t)| \leq V_{PK}^{Adv}$  for all  $t$ : the

<sup>3</sup> Our security definitions of Section IV would consider the attacker successful regardless of the duration of attack. However, to deal with the small drifts in the sampling frequency which cause high-frequency components to re-appear, an attacker could use the techniques introduced in [12].

adversary is only constrained by power budget requirements. Whether or not the adversary succeeds in injecting the target waveform  $w(t)$  into the output of the system depends on the transfer functions  $H_C$  and  $H_A$ . For a given system described by  $H_A$  and  $H_C$ , there are three outcomes against an adversary whose only restriction is power:

- 1) The adversary can disturb the sensor readings, but cannot precisely control the measurement outputs, an attack we call *existential injection*. The lack of existential injections can be considered *universal security*.
- 2) The adversary can inject a target waveform  $w(t)$  into the ADC outputs with high fidelity, performing a *selective injection*. If the adversary is unable to succeed, the system is *selectively secure* against  $w(t)$ .
- 3) The adversary can *universally inject* any waveform  $w(t)$ . If there is any non-trivial waveform for which the adversary fails, the system is *existentially secure*.

This section sets out to precisely define the above security notions by accounting for noise and quantization error (Equation (1)). Our definitions capture the intuition that systems are secure when there are no adversarial transmissions, and are “monotonic” in power, i.e., systems are more vulnerable against adversaries with access to higher-powered transmitters. Our definitions are also monotonic in noise. In other words, in environments with low noise, even a small disturbance of the output is sufficient to break the security of a system. Section IV-A evaluates whether an adversary can disturb the ADC output away from its correct value sufficiently. Section IV-B then formalizes the notion of selective security against target waveforms  $w(t)$ . Finally, Section IV-C introduces universal injections by defining what a non-trivial waveform is.

#### A. Existential Injection, Universal Security

The most primitive notion of attack is whether an adversary can simply disrupt the sensor readings. There are two axes in which this notion can be evaluated: adversarial power and probability of success.<sup>4</sup> For a fixed probability of success, we want to determine the least amount of power for which an attack is successful. For a fixed power, we want to find the probability of a successful attack. Alternatively, if we fix both power and probability of success, we want to be able to determine if a system is secure against signal injection attacks.

The definition for universal security is a formalization of the above intuition, calling a system secure when, even in the presence of injections (bounded by adversarial power), the analog sensor value and the ADC digital output do not deviate by more than the quantization error and the noise, with sufficiently high probability. Mathematically:

**Definition 1 (Universal Security, Existential Injection):** For  $0 \leq \epsilon < 1$ , and  $V_{PK}^{Adv} \geq 0$ , we call a system **universally**  $(\epsilon, V_{PK}^{Adv})$ -**secure** if

$$Pr \left[ E_s(t) \geq Q + N^{-1} \left( \frac{\epsilon + 1}{2} \right) \right] \leq \frac{\epsilon + 1}{2} \quad (5)$$

<sup>4</sup> Success is probabilistic, as noise is a random variable.

for every adversarial waveform  $v(t)$ , with  $|v(t)| \leq V_{PK}^{Adv}$  for all  $t$ .  $Q$  is the quantization error of the system,  $N^{-1}$  is the noise distribution inverse defined in Equation (2), and  $E_s$  is the sampling error as defined by Equation (3). The probability is taken over the duration of the attack, i.e., at each sampling point within the interval  $t_{start} \leq t \leq t_{end}$ . We call a successful attack an **existential injection**, and simply call a system universally  $\epsilon$ -secure, when  $V_{PK}^{Adv}$  is clear in context.

We first show that in the absence of injections, the system is universally  $\epsilon$ -secure for all  $0 \leq \epsilon < 1$ . Indeed, let  $x = N^{-1} \left( \frac{\epsilon + 1}{2} \right)$ , so that  $Pr [ |n(t)| \leq x ] = \frac{\epsilon + 1}{2}$ . Then, in the absence of injections,

$$\begin{aligned} Pr \left[ E_s(t) \geq Q + N^{-1} \left( \frac{\epsilon + 1}{2} \right) \right] &= Pr [ |n(t)| \geq x ] = \\ &= 1 - \frac{\epsilon + 1}{2} = \frac{1 - \epsilon}{2} \leq \frac{\epsilon + 1}{2} \end{aligned}$$

which holds for all  $0 \leq \epsilon < 1$ , as desired. This proof is precisely the reason for requiring a noise level and probability of at least 50% in the definition: the proof no longer works if  $(1 + \epsilon)/2$  is replaced by just  $\epsilon$ . In other words, mere noise would be classified as an attack by the modified definition.

**Power:** We now show that a higher adversarial power budget can only make the system more vulnerable. Indeed, if a system is universally  $(\epsilon, V_1)$ -secure, then it is universally  $(\epsilon, V_2)$ -secure for  $V_2 \leq V_1$ . For this, it suffices to prove the contrapositive, i.e., that if a system is not universally  $(\epsilon, V_2)$ -secure, then it is not universally  $(\epsilon, V_1)$ -secure. For the proof, let  $v(t)$  be an adversarial waveform with  $|v(t)| \leq V_2$  such that Equation (5) does not hold, which exists by the assumption that the system is not universally  $(\epsilon, V_2)$ -secure. Then, by the transitive property,  $|v(t)| \leq V_1$ , making  $v(t)$  a valid counterexample for universal  $(\epsilon, V_1)$  security, as desired.

**Probability:** The third property we show is probability monotonicity, allowing us to define a “critical threshold” for  $\epsilon$ , above which a system is universally secure (for a fixed  $V_{PK}^{Adv}$ ), and below which a system is not universally secure. Indeed, for fixed  $V_{PK}^{Adv}$ , if a system is universally  $(\epsilon, V_{PK}^{Adv})$ -secure, then it is universally  $(\epsilon + \delta, V_{PK}^{Adv})$ -secure for  $0 \leq \delta < 1 - \epsilon$ , as

$$\begin{aligned} Pr \left[ E_s(t) \geq Q + N^{-1} \left( \frac{\epsilon + \delta + 1}{2} \right) \right] &\leq \\ Pr \left[ E_s(t) \geq Q + N^{-1} \left( \frac{\epsilon + 1}{2} \right) \right] &\leq \frac{\epsilon + 1}{2} \leq \frac{\epsilon + \delta + 1}{2} \end{aligned}$$

because  $N^{-1}$  is increasing. The contrapositive is, of course, also true: if a system is not universally secure for a given  $\epsilon$ , it is also not universally secure for  $\epsilon - \delta$  with  $0 \leq \delta \leq \epsilon$ .

**Thresholds:** For a given security level  $\epsilon$ , then, we can talk about the maximum (if any)  $V_{PK}^{Adv}$  such that a system is universally  $(\epsilon, V_{PK}^{Adv})$ -secure, or conversely the minimum (if any)  $V_{PK}^{Adv}$  such that a system is not universally  $(\epsilon, V_{PK}^{Adv})$ -secure. This is the **critical universal voltage level**  $V_c$  for the given  $\epsilon$ . Moreover, for any  $V_{PK}^{Adv}$ , there is a unique **critical universal security threshold**  $\epsilon_c$  such that the system is universally  $(\epsilon, V_{PK}^{Adv})$ -secure for  $\epsilon_c < \epsilon < 1$  and not universally  $(\epsilon, V_{PK}^{Adv})$ -secure for  $0 \leq \epsilon < \epsilon_c$ . By convention

we take  $\epsilon_c = 0$  if the system is secure for all  $\epsilon$ , and  $\epsilon_c = 1$  if there is no  $\epsilon$  for which the system is secure. This critical threshold indicates the security level of a system: the lower  $\epsilon_c$ , the better a system is protected against signal injection attacks.

### B. Selective Injection and Security

The second definition captures the notion of security against specific target waveforms  $w(t)$ : we wish to find the probability that a  $V_{PK}^{Adv}$ -bounded adversary can make  $w(t)$  appear in the output of the ADC. Conversely, to define security in this context, we must make sure that the digitized signal  $\tilde{s}_f(t)$  differs from the waveform  $s(t) + w(t)$  with high probability, even if plenty of noise is allowed. There are two crucial points to notice about the waveform  $w(t)$ . First,  $w(t)$  is not the raw signal  $v(t)$  the adversary is transmitting, as this signal undergoes two transformations via  $H_C$  and  $H_A$ . Instead,  $w(t)$  is the signal that the adversary wants the ADC to think that it is seeing, and is usually a demodulated version of  $v(t)$  (see Figure 1). Second,  $w(t)$  does not necessarily cancel out or overpower  $s(t)$ , because that would require predictive modeling of the sensor signal  $s(t)$ . However, if the adversary can predict  $s(t)$  (e.g., by monitoring the output of the ADC, or by using identical sensors), we can then ask about security against the waveform  $w'(t) = w(t) - s(t)$  instead. Given this intuition, we can define selective security as follows:

*Definition 2 (Selective Security, Selective Injection):* For  $0 \leq \epsilon < 1$ , and  $V_{PK}^{Adv} \geq 0$ , a system is called **selectively**  $(\epsilon, w(t), V_{PK}^{Adv})$ -**secure** if

$$\Pr \left[ E_{s+w}(t) \geq Q + N^{-1} \left( \frac{(1-\epsilon)+1}{2} \right) \right] > \frac{2-\epsilon}{2} \quad (6)$$

for every adversarial waveform  $v(t)$ , with  $|v(t)| \leq V_{PK}^{Adv}$  for all  $t$ , where the probability is taken over the duration of the attack.  $Q$  is the quantization error of the system,  $N^{-1}$  is the noise distribution inverse defined in Equation (2), and  $E_{s+w}(t) = |\tilde{s}_f(t+\tau) - s(t) - w(t)|$  during sampling periods, and 0 otherwise. We call a successful attack a **selective injection**, and simply call a system selectively  $\epsilon$ -secure, when  $V_{PK}^{Adv}$  and  $w(t)$  are clear from context.

As before, our definition is monotonic in both the adversarial power, and the probability of success, allowing us to talk about “the” probability of success for a given waveform:

**Power:** The same argument as in the previous section shows that increasing  $V_{PK}^{Adv}$  can only make a secure system insecure, but not vice versa, i.e., that if a system is selectively  $(\epsilon, w(t), V_1)$ -secure, then it is selectively  $(\epsilon, w(t), V_2)$ -secure for  $V_2 \leq V_1$ . We can thus again define the **critical selective voltage level**  $V_c^w$  for a given  $\epsilon$  and  $w(t)$ .

**Probability:** If a system is selectively  $\epsilon$ -secure (against a target waveform and power budget), then it is selectively  $(\epsilon + \delta)$ -

secure for  $0 \leq \delta < 1 - \epsilon$ , because

$$\begin{aligned} P &= \Pr \left[ E_{s+w}(t) \geq Q + N^{-1} \left( \frac{1 - (\epsilon + \delta) + 1}{2} \right) \right] \\ &\geq \Pr \left[ E_{s+w}(t) \geq Q + N^{-1} \left( \frac{1 - \epsilon + 1}{2} \right) \right] \\ &> \frac{2 - \epsilon}{2} \geq \frac{2 - (\epsilon + \delta)}{2} \end{aligned}$$

Similarly, if the system is not selectively  $\epsilon$ -secure, then it is not selectively  $(\epsilon - \delta)$ -secure.

Given the above properties, for a given waveform  $w(t)$  and fixed  $V_{PK}^{Adv}$ , we can define a waveform-specific **critical selective security threshold**  $\epsilon_c^w$  such that the system is vulnerable for all  $\epsilon^w$  with  $0 \leq \epsilon^w < \epsilon_c^w$  and secure for all  $\epsilon^w$  with  $\epsilon_c^w < \epsilon^w < 1$ . As before, by convention, we take  $\epsilon_c^w = 0$  if there is no  $\epsilon$  for which the system is vulnerable, and  $\epsilon_c^w = 1$  if there is no  $\epsilon$  for which the system is secure.

**Threshold Relationship:** The critical universal threshold of a system  $\epsilon_c$  is related to the critical selective threshold  $\epsilon_c^0$  against the zero waveform  $w(t) = 0$  through the equation  $\epsilon_c^0 = 1 - \epsilon_c$ . Indeed, if a system is not universally  $\epsilon$ -secure, then  $P = \Pr [E_s(t) \geq Q + N^{-1} (\frac{\epsilon+1}{2})] > \frac{\epsilon+1}{2}$ , so  $\Pr [E_{s+0}(t) \geq Q + N^{-1} (\frac{(1-(1-\epsilon))+1}{2})] = P > \frac{(1-(1-\epsilon))+1}{2} = \frac{2-(1-\epsilon)}{2}$ , so the system is selectively  $(1 - \epsilon)$ -secure for the zero waveform. Conversely, if a system is selectively  $(1 - \epsilon)$ -secure for the zero waveform, then it is not universally  $\epsilon$ -secure. The fact that a low critical universal threshold results in a high critical selective threshold for the zero threshold is not surprising: it is easy for an adversary to inject a zero signal by simply not transmitting anything.

### C. Universal Injection, Existential Security

The final notion of security is a weak one, which requires that the adversary cannot inject at least one “representable” waveform into the system, i.e., one which is within the ADC limits. We can express this more precisely as follows:

*Definition 3 (Representable Waveform):* A waveform  $w(t)$  is called **representable** if it is within the ADC voltage levels, and has a maximum frequency component bounded by the Nyquist frequency of the ADC. Mathematically,  $V_{min} \leq w(t) \leq V_{max}$  and  $f_{max} \leq f_s/2$ .

Using this definition, we can introduce security against at least one representable waveform:

*Definition 4 (Existential Security, Universal Injection):* For  $0 \leq \epsilon < 1$ , and  $V_{PK}^{Adv} \geq 0$ , a system is called **existentially**  $(\epsilon, V_{PK}^{Adv})$ -**secure** if there exists a representable waveform  $w(t)$  for which the system is selectively  $(\epsilon, w(t), V_{PK}^{Adv})$ -secure. We will call a system existentially  $\epsilon$ -secure when  $V_{PK}^{Adv}$  is clear from context. If there is no such  $w(t)$ , we say that the adversary can perform any **universal injection**.

As in previous definitions, power and probability are monotonic in the opposite direction.

**Power:** If a system is existentially  $(\epsilon, V_1)$ -secure, then it is  $(\epsilon, V_2)$ -secure for  $V_2 \leq V_1$ . By assumption, there is a representable  $w(t)$  such that the system is selectively  $(\epsilon, w(t), V_1)$ -

secure. By the previous section, this system is  $(\epsilon, w(t), V_2)$ -secure, concluding the proof.

**Probability:** If a system is existentially  $(\epsilon_1, V)$ -secure, then it is  $(\epsilon_2, V)$ -secure for  $\epsilon_1 \leq \epsilon_2$ . By assumption, there is a representable  $w(t)$  such that the system is selectively  $(\epsilon_1, w(t), V)$ -secure. By the previous section, the system is also  $(\epsilon_2, w(t), V)$ -secure, as desired.

**Thresholds:** Extending the definitions of the previous sections, for fixed  $\epsilon$  we can define a **critical existential voltage level**  $V_c^{exist}$  below which a system is existentially  $\epsilon$ -secure, and above which the system is existentially  $\epsilon$ -insecure. Similarly, for a fixed adversarial voltage we can define the **critical existential security threshold**  $\epsilon_c^{exist}$ , above which the system is existentially secure, and below which the system is insecure.

Although existential security might seem easy to accomplish, if the circuit-specific transfer function  $H_C$  is the identity, the system is not even existentially secure. In other words, if  $H_C$  does not transform inputs (as in some of the experiments in Section III), an adversary can simply directly transmit  $v(t) = w(t)$  unmodulated.  $w(t)$  will then appear at the output of the ADC, allowing an adversary to perform a universal injection attack.

In other contexts, security designers may wish to adjust the definitions to restrict target waveforms (and hence existential security counterexamples) even further. For instance, we might wish to check whether an adversary can inject all waveforms which are sufficiently bounded away from 0, or all sinusoidal waveforms of a specific frequency. The proofs for power and probability monotonicity still hold, allowing us to talk about universal security against  $\mathcal{S}$ -representable waveforms: waveforms which are representable and also in a set  $\mathcal{S}$ .

## V. SECURITY IN PRACTICE:

### A SMARTPHONE MICROPHONE CASE STUDY

In this section, we illustrate how our security definitions can be used to determine the security level of a commercial, off-the-shelf smartphone microphone. We first introduce an algorithm to calculate the critical selective security threshold  $\epsilon_c^w$  against a target waveform  $w(t)$  in Section V-A. We then use the algorithm to calculate the critical thresholds of a smartphone in Section V-B. Finally, we comment on universal security in Section V-C, where we characterize the phone’s behavior across a range of different carrier frequencies and show that we are able to inject complex “OK Google” commands. We summarize our results in Table II.

#### A. Algorithm for Selective Security Thresholds

In this section, we introduce an algorithm to calculate the critical selective security threshold  $\epsilon_c^w$  of a system against a target waveform  $w(t)$ , using a transmitted signal  $v(t)$ . The first step in calculating the security level is determining the noise distribution. To that end, we collect  $N$  measurements of the system output  $\tilde{s}_f(t)$  during the injection and pick one as the *reference* signal. We then pick  $1 \leq k \leq N - 2$  of them to calculate the noise (*estimation* signals), while the remaining are used to verify our calculations (*validation* signals).

Injection	Resulting Signal	Crit. Thres.
Existential	$w(t) \neq 0$	0.892
Selective	$w(t) = e^{\sin(2\pi f_m t)}$	0.747
Selective	$w(t) = \sin(2\pi f_m t)$	0.562
Universal	“OK Google” commands	$\leq 0.562$

TABLE II: The adversary can easily disturb the smartphone output (existential injection), and inject human speech (universal injection). Selective injections of sines are less precise than exponentials of the same frequency.

Our algorithm first removes any DC offset and re-scales the measurements so that the root-mean-square (RMS) voltages of the signals are the same. The repeated measurements are then phase-aligned, and we calculate the distance between the reference signal and the estimation signals. The average of this distance should be very close to 0, as the signals are generated in the same way. However, the standard deviation  $\sigma$  is non-zero, so we can model noise as following a zero-mean normal distribution  $n(t) \sim N(0, \sigma^2)$ . We can then find the critical threshold between the reference signal and any target *ideal* waveform  $w(t)$  as follows: we first detrend, scale, and align the ideal signal to the reference waveform, as with the estimation signals. Then, we calculate the errors (distance) between the ideal and the reference signal. Finally, we perform a binary search for different values of  $\epsilon$ , in order to find the largest  $\epsilon$  for which Equation (6) does not hold: this is the critical threshold. To calculate the inverse of the noise, we use the percentile point function  $ppf(\epsilon)$ , which is the inverse of the cumulative distribution function, and satisfies  $N^{-1}(\epsilon) = ppf((1 + \epsilon)/2)$ .

Note that since the critical universal threshold  $\epsilon_c$  is related to the selective critical threshold of the zero waveform  $\epsilon_c^0$  through  $\epsilon_c = 1 - \epsilon_c^0$  (Section IV-B), the same algorithm can be used to calculate  $\epsilon_c$ . Our algorithm is summarized in pseudocode as Algorithm 1.

#### B. Existential and Selective Injections of a Smartphone

We demonstrate how our algorithm can be used in a realistic setup using a Motorola XT1541 Moto G3 smartphone. We inject modulated  $f_m = 1$  kHz signals, collecting  $N = 10$  measurements of  $2^{15}$  sample points per run, and record the data at a frequency of  $f_s = 44.1$  kHz. We first modulate  $f_m$  over  $f_c = 200$  MHz using an output level of  $V_{RMS}^{Adv} = 0.2$  V. This injection is demodulated well by the smartphone and has a similarity of over 0.98 compared to the pure 1 kHz tone. We call this example the “clean” waveform. The second injection, which we call the “distorted” waveform, uses  $f_c = 25$  MHz,  $V_{RMS}^{Adv} = 0.9$  V, and has a similarity of less than 0.55 to the ideal tone. Example measurements of these signals and “ideal” signals (see below) are shown in Figure 9.

The algorithm first calculates the noise level using the reference signals. As expected, the error average is very close to 0 (usually less than  $10^{-6}$ ), while, the standard deviation  $\sigma$  is noticeable at around 0.0015. Taking the reference signals as the target signal  $w(t)$ , the critical thresholds were always close to 1. In other words, even if the injected waveforms do not correspond to a “pure” signal, the adversary can inject them

---

**Algorithm 1** How to Calculate the Critical Selective Security Threshold
 

---

```

1: procedure FIND_CRITICAL_EPSILON(measured, ideal, sigma)
2:   errors  $\leftarrow$   $|measured - ideal|/sigma$ 
3:   lo  $\leftarrow$  0.5
4:   hi  $\leftarrow$  1
5:   while lo < hi do
6:     mid  $\leftarrow$  (lo + hi)/2
7:     ninv  $\leftarrow$  ppf((1 + mid)/2)
8:     perror  $\leftarrow$  length( $[x \geq n_{inv} : x \in errors]$ )/length(errors)
9:     if  $|p_{error} - mid| < 10^{-4}$  & perror  $\leq$  mid then
10:      return  $2 - 2 * mid$ 
11:     else if perror < mid then
12:       hi  $\leftarrow$  mid
13:     else
14:       lo  $\leftarrow$  mid
15: procedure COMPARE(measurements, ideal)
16:   ref  $\leftarrow$  detrend(measurements[0])
17:   estimating  $\leftarrow$  align(scale(detrend(measurements[1 : ]), ref), ref)
18:   errors  $\leftarrow$  (measured - ref)  $\forall$  measured  $\in$  estimating
19:    $\sigma_{noise}$   $\leftarrow$  std_deviation(errors)
20:   ideal  $\leftarrow$  align(scale(detrend(ideal), ref), ref)
21:   return Find_Critical_Epsilon(ref, ideal,  $\sigma_{noise}$ )

```

$\triangleright$  Calculate normalized absolute errors  
 $\triangleright$  Probabilities need to be between 0.5 and 1  
 $\triangleright$  *mid* represents  $(2 - \epsilon)/2$   
 $\triangleright$  Percentile point function  
 $\triangleright$  Break out if sufficiently close  
 $\triangleright$  Use repeated *measurements*  
 $\triangleright$  Pick first series as reference, remove DC  
 $\triangleright$  Calculate noise from estimation measurements

---

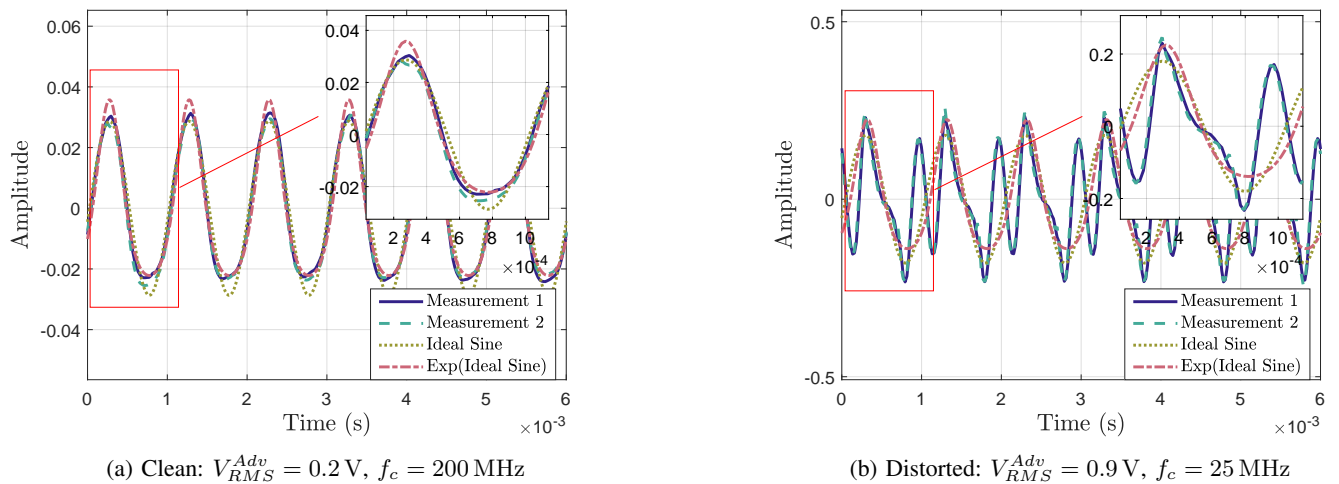


Fig. 9: Waveforms injected into the smartphone, with ideal sine and exponential sine functions for comparison.

with high fidelity: the system is not selectively secure against them with high probability.

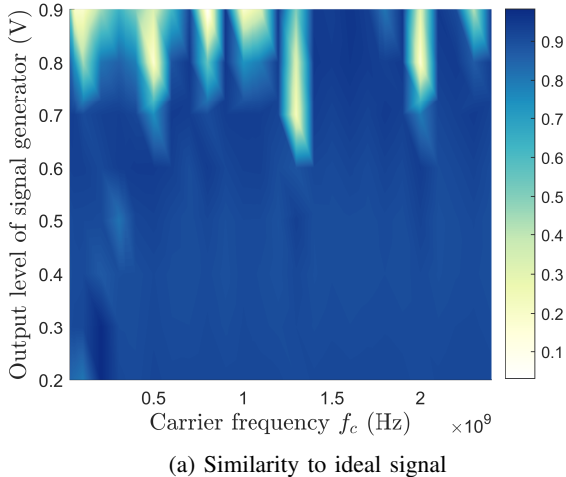
We also tried two signals as the ideal signal that the adversary is trying to inject: a pure 1 kHz sine wave, and an exponential of the same sine wave. The averages and standard deviations for the calculated thresholds over all combinations of  $k$  and reference signals are shown in Table III. As we would expect, the thresholds for the distorted waveform are much lower than the values for the clean waveform: the signal is distorted, so it is hard to inject an ideal signal. We also find that the exponential function is a better fit for the signal we are seeing, and can better explain the harmonics. Table III also includes the critical universal injection threshold based on the two waveform injections. This threshold is much higher for both waveforms, as injections disturb the ADC output sufficiently, even when the demodulated signal is not ideal.

Waveform	Validation	Ideal Sine	$\epsilon_c^{\text{Ideal Sine}}$	$w(t) \neq 0$
Clean	(0.98, 0.03)	(0.56, 0.04)	(0.75, 0.06)	(0.89, 0.01)
Distorted	(0.95, 0.09)	(0.31, 0.05)	(0.34, 0.05)	(0.71, 0.04)

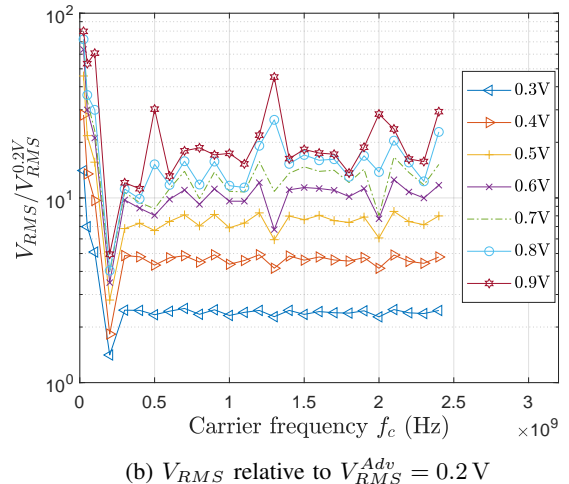
TABLE III: Mean and std. deviation ( $\mu, \sigma$ ) of critical selective thresholds  $\epsilon_c^w$  for different target signals  $w(t)$  for the two waveforms of Figure 9. Injections using the clean waveform are always more successful than with the distorted waveform. Validation signals are injected with high fidelity, and are better represented by an exponential rather than a pure sine.

### C. Universal Injections on a Smartphone

In this section, we investigate the existential security of the smartphone by characterizing its ADC's behavior across a range of carrier frequencies. We show that the non-linearities in the smartphone's analog frontend can be mathematically predicted using models from the literature. We finally demon-



(a) Similarity to ideal signal



(b)  $V_{RMS}$  relative to  $V_{RMS}^{Adv} = 0.2\text{ V}$

Fig. 10: Similarity of demodulated smartphone injections compared to the ideal signal (10a) and relative received RMS voltage  $V_{RMS}$  (10b) for different output voltage levels  $V_{RMS}^{Adv}$  and carrier frequencies  $f_c$ .

strate that the smartphone is vulnerable to the injection of arbitrary “OK Google” commands, which cause the smartphone to behave as if the user initiated an action.

**Characterization:** We inject a 1 kHz tone that is AM-modulated with a depth of  $m = 100\%$  on the following carrier frequencies  $f_c$ : 25 MHz, 50 MHz, and 100 – 2400 MHz at a step of 100 MHz. We also vary the RMS output level  $V_{RMS}^{Adv} = V_{PK}^{Adv} / \sqrt{2}$  of our signal generator between 0.2–0.9 V at a step of 0.1 V. The similarity of the measured signal compared to the ideal signal for various carrier frequencies  $f_c$  and output levels  $V_{RMS}^{Adv}$  is shown in Figure 10a, and is consistently high for all frequencies when  $0.2\text{ V} \leq V_{RMS}^{Adv} \leq 0.6\text{ V}$ . Higher voltage levels may lead to more pronounced harmonics and clipping, causing the similarity to drop.

Prior work in direct power injections against amplifiers without ADCs [13] suggested the following relationship between the RMS measured level  $V_{RMS}$ , the input power level  $V_{RMS}^{Adv}$ , the modulation depth  $m$ , the signal frequency  $f_m$  and the carrier frequency  $f_c$ :

$$V_{RMS}(V_{RMS}^{Adv}) = \frac{\sqrt{2}}{2} m (V_{RMS}^{Adv})^2 |H_2(f_c, -(f_c - f_m))| \quad (7)$$

where  $H_2$  is a second-order transfer function. We thus expect that if we fix  $m$  and  $f_m$ ,  $V_{RMS}(V_1)/V_{RMS}(V_2) = (V_1/V_2)^2$  across all carrier frequencies  $f_c$ . Figure 10b shows the results of our measurements for  $V_2 = 0.2\text{ V}$ . For  $0.3\text{ V} \leq V_1 \leq 0.6\text{ V}$ , this linear relationship is confirmed for  $f_c \geq 100\text{ MHz}$ , although the relationship for larger  $V_1$  is more noisy, due to distortions. These results show that a higher-order transfer function can be used to accurately predict the ADC output in response to signal injections.

**Command Injection:** While in the previous sections we have been focusing on sinusoidal injections, in this section we show that we can inject arbitrary complex waveforms which are also demodulated by the smartphone. We first injected a recording of “OK Google, turn on the flashlight” modulated at all the

above carrier frequencies  $f_c$  at  $V_{RMS}^{Adv} = 0.6\text{ V}$ . The voice-activation feature (“OK Google”) worked with 100% success rate for all frequencies, and the full command was successfully executed for 23 of the 26 frequencies we tested. Increasing the output level to  $V_{RMS}^{Adv} = 0.9\text{ V}$ , increased success rate to 25/26 frequencies. Only  $f_c = 2.4\text{ GHz}$  did not result in a full command injection, possibly because the Wi-Fi disconnected in the process. Our results remained the same when we changed the command to call and text contacts, set a timer, mute the volume, or turn on airplane mode. We thus found that all carrier frequencies which are not severely attenuated by  $H_C$  (e.g., when coupling to the user’s headphones) are vulnerable to complex signal injections.

## VI. DISCUSSION

The previous sections have shown that direct power injection is a practical way of understanding the ADC response  $H_A$  to high-frequency inputs beyond its sampling frequency: ADCs are vulnerable to modulated signal injections at carrier frequencies much higher than their cutoff frequencies, despite the low-pass filter (LPF) effect of the sample-and-hold mechanism. From the designer’s perspective, choosing the right ADC directly impacts the susceptibility to signal injection attacks. For instance, the ATmega328P and the TLC549 result in more sawtooth-like output compared to the AD7833, and are more resilient to clean sinusoidal injections. By contrast, the output of the remaining 3 ADCs is more sine-like, but requires more fine-grained control over the carrier frequency, which the adversary may not have after the signal has been transformed through the circuit-specific transfer function  $H_C$ .

Having chosen the appropriate ADC based on cost, performance, security, or other considerations, a designer needs to assess the impact of  $H_C$ . Prior work has shown that even small layout or component changes affect the EMI behavior of a circuit [6], [9], [13]. Our approach allows us to decouple these considerations from the ADC behavior, and provides a

clear methodology to find out which types of injections a system is vulnerable to. It also allows designers to quickly evaluate whether a system has become more secure in response to changes in the topology/components of the circuit board.

As our experiments of Section III-B and the related work of Section VII show, remote attacks are feasible, and challenges are primarily engineering in nature. Consequently, there are two questions to answer for any system: (1) what types of waveforms can an adversary inject, and (2) how powerful must the adversary be to do so? Our selective security definition and algorithm address how to determine the vulnerability of a system against specific waveforms. Universal security allows us to evaluate the requirements for successful adversarial attacks in two ways. First, for a fixed adversarial power budget, the security of two systems can be directly compared using the critical universal security threshold. Second, given a probability/threshold  $\epsilon$ , we can calculate the critical universal voltage level, which is the maximum output level for which a system is still universally  $\epsilon$ -secure.

Our case study for the security of a smartphone showed that our model and security definitions can be used in practice to estimate the security level of real systems. Moreover, our “OK Google” experiments demonstrated that less-than-perfect injections of adversarial waveforms can have the same effect as perfect injections. This is because there is a mismatch between the true noise-level of a system and the worst-case noise-level that the system expects. In other words, injections worked at all carrier frequencies, even when the demodulated output was noisy or distorted. This is a deliberate, permissive design decision, which allows the adversary to work with a range of different and noisy waveforms  $w(t)$ . As long as the probability of selective injection is high enough for at least one of them, the adversary can succeed, despite the noisy output, small amplitudes, and DC offsets.

Although not heavily discussed in this paper, our model and definitions are general enough to capture alternative signal injection techniques. For instance, electro-mechanical sensors have resonant frequencies which allow acoustic injection attacks [12], [14].  $H_C$  can account for such imperfections in the sensors themselves, attenuating injection frequencies which are not close to the resonant frequencies. Our system model also makes it easy to evaluate countermeasures and defense mechanisms in its context. For example, shielding increases the attenuation factor of  $H_C$ , thereby increasing the power requirements for the adversary (Section II-A1).

Alternatively, a low-pass filter before the ADC and/or amplifier changes  $H_A$ , and attenuates the high-frequency components which would induce non-linearities. Note, however, that even moving the LNA, LPF and ADC into the same IC package does not fully eliminate the vulnerability to signal injection attacks (Section VII) as the channel between the analog sensor and the ADC cannot be fundamentally authenticated. Future work could investigate whether signal injections could instead be detected in aggregate, for instance by adding jitter to the sampling rate, and then oversampling and analyzing the ADC output for harmonics and high-frequency components.

## VII. RELATED WORK

Related work broadly falls under two different categories: (a) attacking sensors/components using electromagnetic, acoustic, and optical injections; and (b) modeling and attacking ADCs and/or amplifiers. In the former category, Foo Kune et al. [1] injected intentional, low-power, low-frequency (kHz range) EMI signals into implantable medical devices (IMDs), causing them to deliver defibrillation shocks. The same work also targeted webcams and bluetooth headsets by transmitting at their resonant frequencies (hundreds of MHz). [15] more recently proposed an analytical model of electromagnetic induction attacks, focusing on the the magnetic field rather than the electric field. Their experiments induced DC offsets using different carrier frequencies, but not time-dependent signals (hence, there was no use of a sub-carrier frequency). By contrast, our work shows how to experimentally determine the response of different ADCs using direct injection attacks with a focus on inducing specific (dynamic, non-constant) waveforms. We also placed these measurements in the context of a new system/threat model and security definitions independent of the signal injection approach, and proposed an algorithm to calculate security thresholds for real systems.

Shoukry et al. [4] presented an attack against Anti-Lock Braking Systems (ABS) by generating a magnetic field that cancels the real signal, and replacing it by a malicious signal. The same researchers later presented an authentication system for active sensors [16], which depends on non-spoofable physical and computational delay limits. The proposed system was soon broken [17] by exploiting a sampling rate race between the attacker and the victim.

[3] used EMI in order to trigger voice commands in smartphones by emitting AM-modulated signals that get picked up by the user’s hands-free headset. In our work, we more precisely characterized the vulnerability of microphones in smartphones, and used our measurements and model to calculate the critical selective security thresholds of the system. Other researchers have injected voice commands without EMI, through modulating signals on ultrasound frequencies [18], or by playing two tones at different ultrasound frequencies, and exploiting non-linearities in components [19].

Acoustic attacks which transmit sound waves at the resonant frequencies of gyroscopes can incapacitate [14] or precisely control drones [20]. Attackers who account for sampling rate drifts can control the outputs of accelerometers for longer periods of time [12]. Finally, optical attacks can be used to spoof medical infusion pump measurements [21], or to cause autonomous cars and unmanned aerial vehicles (UAVs) to drift or fail [22], [23], [24].

Research into attacks against ADCs has primarily focused on silicon-level attacks [25], [26], while ADC modeling is more concerned with signals which are slower than the Nyquist frequency [27]. Research into EMC compatibility has also investigated the susceptibility of microcontroller I/O pins and ADCs to Direct Power Injection (DPI) [28], [29],

[30], [31], [32], [33]. Such research has found that as the frequency of the input increases, immunity to DPI also increases: higher frequencies generally require higher forward power injections for the same level of susceptibility. Such work is more concerned with the average power received, but our experiments focus on the demodulation properties of ADCs. We experimented with all major types of ADCs and characterized the similarity of the measured signal to the ideal signal. Our approach is thus more similar to research into demodulation characteristics of amplifiers [13], [34]. As a result, it can be complemented via mathematical modeling, as, for instance, in [9].

## VIII. CONCLUSION

Sensors guide many of our choices, and we often blindly trust their values. However, it is possible to spoof their outputs through electromagnetic or other types of signal injection attacks. To address the lack of a unifying framework describing the susceptibility of devices to such attacks, we defined a system and adversary model for signal injections. Our model is the first to abstract away from specific environments and circuit designs and presents a strong adversary who is only limited by transmission power. It also makes it easy to discuss and evaluate countermeasures in its context and is general enough to cover different types of signal injection attacks.

Within our model, we defined existential, selective, and universal security, capturing effects ranging from mere disruptions of the ADC outputs to precise injections of all waveforms. We showed in practice that our definitions can be used to evaluate the security level of real systems, and we introduced a novel algorithm to calculate “critical” thresholds, which express how close the injected signal is to the ideal signal.

Our experiments on ADCs of different properties showed that non-linearities in the ADC components demodulate amplitude-modulated (AM) signals. All ADCs were vulnerable to signal injections, though some required more finely-tuned carrier frequencies. Our experiments with a smartphone showed that other ADCs are vulnerable at all carrier frequencies, something which we exploited to cause the smartphone to respond to arbitrary “OK Google” commands. In response to the emerging signal injection threat, our work paves the way towards a future where security can be quantified and compared through our methodology and security definitions.

## REFERENCES

- [1] D. F. Kune, J. D. Backes, S. S. Clark, D. B. Kramer, M. R. Reynolds, K. Fu, Y. Kim, and W. Xu, “Ghost talk: Mitigating EMI signal injection attacks against analog sensors,” in *IEEE Symposium on Security and Privacy (S&P)*, 2013.
- [2] K. Fu and W. Xu, “Risks of trusting the physics of sensors,” *Commun. ACM*, vol. 61, no. 2, pp. 20–23, 2018.
- [3] C. Kasmi and J. L. Esteves, “IEMI threats for information security: Remote command injection on modern smartphones,” *IEEE Transactions on Electromagnetic Compatibility*, vol. 57, no. 6, pp. 1752–1755, 2015.
- [4] Y. Shoukry, P. D. Martin, P. Tabuada, and M. B. Srivastava, “Non-invasive spoofing attacks for anti-lock braking systems,” in *Cryptographic Hardware and Embedded Systems (CHES)*, 2013.
- [5] M. Leone and H. L. Singer, “On the coupling of an external electromagnetic field to a printed circuit board trace,” *IEEE Transactions on Electromagnetic Compatibility*, vol. 41, no. 4, pp. 418–424, 1999.
- [6] A. Lissner, E. Hoene, B. Stube, and S. Guttowski, “Predicting the influence of placement of passive components on EMI behaviour,” in *European Conference on Power Electronics and Applications*, 2007.
- [7] M. J. M. Pelgrom, *Analog-to-Digital Conversion*, 3rd ed. Springer Publishing Company, Incorporated, 2017.
- [8] J.-M. Redouté and M. Steyaert, *EMC of Analog Integrated Circuits*, 1st ed. Springer Publishing Company, Incorporated, 2009.
- [9] J. Gago, J. Balcells, D. González, M. Lamich, J. Mon, and A. Santolaria, “EMI susceptibility model of signal conditioning circuits based on operational amplifiers,” *IEEE Transactions on Electromagnetic Compatibility*, vol. 49, no. 4, pp. 849–859, 2007.
- [10] J. Benesty, J. Chen, and Y. Huang, “On the importance of the Pearson correlation coefficient in noise reduction,” *IEEE Transactions on Audio, Speech, and Language Processing*, vol. 16, no. 16, pp. 757–765, 2008.
- [11] P. D. Lena and L. Margara, “Optimal global alignment of signals by maximization of Pearson correlation,” *Information Processing Letters*, vol. 110, no. 16, pp. 679–686, 2010.
- [12] Y. Tu, Z. Lin, I. Lee, and X. Hei, “Injected and delivered: Fabricating implicit control over actuation systems by spoofing inertial sensors,” in *USENIX Security Symposium*, 2018.
- [13] Y. H. Sutu and J. J. Whalen, “Statistics for demodulation RFI in operational amplifiers,” in *International Symposium on Electromagnetic Compatibility (EMC)*, 1983.
- [14] Y. Son, H. Shin, D. Kim, Y. Park, J. Noh, K. Choi, J. Choi, and Y. Kim, “Rocking drones with intentional sound noise on gyroscopic sensors,” in *USENIX Security Symposium*, 2015.
- [15] J. Selvaraj, G. Y. Dayanikli, N. P. Gaunkar, D. Ware, R. M. Gerdes, and M. Mina, “Electromagnetic induction attacks against embedded systems,” in *Asia Conference on Computer and Communications Security (ASIACCS)*, 2018.
- [16] Y. Shoukry, P. Martin, Y. Yona, S. Diggavi, and M. Srivastava, “PyCRA: Physical challenge-response authentication for active sensors under spoofing attacks,” in *Conference on Computer and Communications Security (CCS)*, 2015.
- [17] H. Shin, Y. Son, Y. Park, Y. Kwon, and Y. Kim, “Sampling race: Bypassing timing-based analog active sensor spoofing detection on analog-digital systems,” in *USENIX Workshop on Offensive Technologies (WOOT)*, 2016.
- [18] G. Zhang, C. Yan, X. Ji, T. Zhang, T. Zhang, and W. Xu, “DolphinAttack: Inaudible voice commands,” in *Conference on Computer and Communications Security (CCS)*, 2017.
- [19] N. Roy, H. Hassanieh, and R. Roy Choudhury, “BackDoor: Making microphones hear inaudible sounds,” in *International Conference on Mobile Systems, Applications, and Services (MobiSys)*, 2017.
- [20] T. Trippel, O. Weisse, W. Xu, P. Honeyman, and K. Fu, “WALNUT: Waging doubt on the integrity of MEMS accelerometers with acoustic injection attacks,” in *IEEE European Symposium on Security and Privacy (EuroS&P)*, 2017.
- [21] Y.-S. Park, Y. Son, H. Shin, D. Kim, and Y. Kim, “This ain’t your dose: Sensor spoofing attack on medical infusion pump,” in *USENIX Workshop on Offensive Technologies (WOOT)*, 2016.
- [22] J. Petit, B. Stottelaar, M. Feiri, and F. Kargl, “Remote attacks on automated vehicles sensors: Experiments on camera and LiDAR,” *Black Hat Europe*, 2015.
- [23] D. Davidson, H. Wu, R. Jellinek, V. Singh, and T. Ristenpart, “Controlling UAVs with sensor input spoofing attacks,” in *USENIX Workshop on Offensive Technologies (WOOT)*, 2016.
- [24] C. Yan, W. Xu, and J. Liu, “Can you trust autonomous vehicles: Contactless attacks against sensors of self-driving vehicle,” *DEFCON*, 2016.
- [25] S. Taheri and J.-S. Yuan, “Mixed-signal hardware security: Attacks and countermeasures for  $\Delta\Sigma$  ADC,” *Electronics*, vol. 6, no. 3, 2017.
- [26] S. Taheri, J. Lin, and J.-S. Yuan, “Security interrogation and defense for SAR analog to digital converter,” *Electronics*, vol. 6, no. 2, 2017.
- [27] K. Folkesson, “ADC modeling for system simulation,” Ph.D. dissertation, Linköping University, 2003.
- [28] A. Boyer, S. Bendhia, and E. Sicard, “Modelling of a direct power injection aggression on a 16 bit microcontroller input buffer,” in *International Workshop on Electromagnetic Compatibility of Integrated Circuit*, 2007.
- [29] F. Lafon, F. D. Daran, M. Ramdani, R. Perdriau, and M. Drissi, “Immunity modeling of integrated circuits: An industrial case,” *Transactions on Communications*, vol. E93.B, no. 7, pp. 1723–1730, 2010.

- [30] X.-l. Gao, C.-y. Tian, L.-y. Lao, Y.-h. Chen, and Y.-y. Chen, "Improved direct power injection model of 16-bit microcontroller for electromagnetic immunity prediction," *Journal of Central South University of Technology*, vol. 18, no. 6, pp. 2031–2035, 2011.
- [31] A. Ayed, T. Dubois, J.-L. Levant, and G. Duchamp, "Failure mechanism study and immunity modeling of an embedded analog-to-digital converter based on immunity measurements," *Microelectronics Reliability*, vol. 55, no. 9, pp. 2067–2071, 2015.
- [32] —, "Immunity measurement and modeling of an ADC embedded in a microcontroller using RFIP technique," *IEEE Transactions on Electromagnetic Compatibility*, vol. 57, no. 5, pp. 955–962, 2015.
- [33] S. Kennedy, M. R. Yuce, and J.-M. Redouté, "Susceptibility of flash ADCs to electromagnetic interference," *Microelectronics Reliability*, vol. 81, pp. 218–225, 2018.
- [34] H. Ghadamabadi, J. J. Whalen, R. Coslick, C. Hung, T. Johnson, W. Sitzman, and J. Stevens, "Comparison of demodulation RFI in inverting operational amplifier circuits of the same gain with different input and feedback resistor values," in *International Symposium on Electromagnetic Compatibility (EMC)*, 1990.